Technical Article

Higher-Order Non-standard FDTD Schemes in Generalised Curvilinear Coordinates – A Systematic Strategy for Advanced Numerical Modeling and Consistent Topological Perspectives

Abstract – An advanced higher-order Finite-Difference Time-Domain (FDTD) method for the accurate solution of complex electromagnetic field problems is developed in this paper. Establishing an essentially algebraic covariant/contravariant approach to the discretisation of the curvilinear div-curl problem, the new technique introduces a generalised set of non-standard operators that fits the exterior calculus of differential forms and their discrete counterparts (cochains). Therefore, the physical properties of Maxwell's laws are precisely assessed, without the need of artificial constraints or lattice reflections, whereas the termination of unbounded domains is performed via optimally designed Perfectly Matched Layers (PMLs). For the temporal variable, the proposed method employs a multi-stage leapfrog integration that guarantees stability and excitation universality. Numerical investigation demonstrates that the proposed methodology accomplishes highly precise simulations, evades late time-instabilities and provides an overwhelming suppression of dispersion or dissipation errors.

Introduction

The successful development and popularity of a numerical procedure in the demanding area of computational electromagnetics depends on a multitude of modeling perspectives whose primary objective is to preserve the fundamental structure of the physical problem under investigation. Among them, we can indicatively discern the discretisation consistency, the strict mathematical robustness, the high accuracy and the well-posed reciprocity profile; issues that additionally guarantee the correct construction of infinitely divisible space-time lattices and bridge the gap between the continuous and discrete state. As a matter of fact, the above stipulations, along with the thriving advances in computer facilities, constitute the essential guidelines for the ongoing evolution of several broadly-acknowledged numerical techniques, such as the Finite Element [1]-[2], the Edge Element [1]-[3], the Finite Integration [4]-[5], the Transmission Line Modeling [6] and the Finite-Difference Time-Domain (FDTD) [7]-[8] method. Concentrating on the solution of Maxwell's equations in the time domain, one can easily ascertain the dominant impact of the FDTD scheme, which since its inceptive advent has established formidable (if not aspiring) modeling goals and radically advanced simulation standards.

Notwithstanding its algorithmic elegance and routine feasibility, the classical FDTD method presents a principal hindrance: its inability to successfully cope with abrupt curvatures and complicated geometries in open-region problems. This innately involved deficiency is proven to be critical, since it renders the well-known "staircasing" procedure inadequate to provide consistent numerical simulations and generates severe discretisation and lattice reflection errors. As the original Yee's approach encompasses a linear mapping to unbounded grids with respect to overall burden, any effort concerning space minimisation is very expedient. Furthermore, the technique's second-order differencing regime, especially on non-orthogonal meshes, is basically answerable to longer execution time and consecutively lower-rates of convergence. Actually, for 3-D structures, the truncation error is manifested in dissipative, dispersive and anisotropic behaviour. Bearing in mind that these vector parasites stem primarily from the improper discrete representation of the unknown field quantities in Maxwell's div-curl equations, it is evident that the FDTD approximation framework should be thoroughly reconsidered. In particular, the use of vector calculus as the basic tool for the extraction of general models, embedded in unstructured meshes, seems to be insufficient, since the resulting forms depend on the underlying coordinate system. Moreover, vector analysis requires that the whole FDTD discretisation strategy must be strongly related to the set of metrics in terms of which the respective continuum field theory is described. Thus, the geometrical attributes and the metric independence of Maxwell's laws remain totally unexplored, while during the construction of the dual-character lattices the centres of primary cells may not coincide with the middle point of any secondary edge, spoiling so the staggered philosophy of the method.

As anticipated, the previous abstractions motivated the introduction of various efficient non-orthogonal FDTD techniques, extensively reviewed in [8]. According to their specific topics, these approaches mainly launch second-order curvilinear schemes applied to diverse scattering, radiation, waveguide and microstrip problems [9]-[15]. Sharing the fundamental notion of consistent cell interfaces, all methods contemplate diverse feasible accuracy enhancements associated with the appropriate FDTD elements in order to manipulate every difficult curvature. Nonetheless, serious attention has been also drawn towards the reflectionless termination of every unbounded domain encountered in the aforementioned applications. Consequently, scientific research concentrated on the extension of existing absorbing boundary conditions (ABCs) to the most frequently-utilised curvilinear coordinate systems. Among the multitude of ABCs, the perfectly matched layer (PML) [16] exhibits the best wave-annihilating characteristics for a wide range of structures. Its prevalent merits became immediately the subject of intensive studies which led to its successful development in cylindrical and spherical coordinates [17]-[18]. Mainly, based on the theory of complex coordinate stretching, these absorbers follow a diagonally anisotropic tensorial formulation in order to circumvent the original split-field (non-Maxwellian) rationale [19]-[21].

However, extensive investigations revealed that the second-order nature of the foregoing techniques can still comprise a serious obstacle for various demanding situations. More spe-

cifically, the inherent discretisation errors may contaminate the results and damage the overall simulation. Hence, the perspective for a firm and straightforward FDTD-PML procedure, able to precisely cope with such deficiencies, remains a challenging quest. It is the purpose of this paper to introduce a generalised higher-order FDTD methodology – founded on advanced non-standard concepts – for the systematic and accurate analysis of intricate 3-D electromagnetic problems established in curvilinear, fully non-orthogonal coordinate systems. Implementing, the language of differential geometry and algebraic topology, the unifying framework achieves the consistent transition from the continuous to lattice state and enables the unperturbed separation of the physical field laws into topological equations (namely, invariant under homeomorphisms) and metric equations which involve the familiar Hodge star operators. Therefore, unlike previous realisations, differential forms and their discrete higher-order counterparts guarantee the natural interaction between field constituents and the rigorous satisfaction of the divergence-preserving relationships. Moreover, the proposed algorithm reveals that numerical schemes, complying with the above specifications, can be naturally conveyed in terms of integrated field quantities related to the computational domain and the notion of dual space-time grids. These assertions along with the fact that the validity of the discrete equations does not depend on the materials occupying the diverse grid regions, allow an alternative updating philosophy that evades unconditional late-time instabilities.

The key premise of the method lies on the representation of electromagnetic fields via a modified higher-order non-standard covariant and contravariant strategy that originates from an efficient treatment of the strenuous div-curl problem. Particularly, its scrupulous solution in any Euclidean space leads to the construction of reflectionless PMLs, whose additional degrees of design freedom and their optimal establishment accomplish a critical attenuation of the outgoing and evanescent waves. Due to the notable reduction of lattice errors in curvilinear domains, higher-order PMLs can handle rapidly increasing artificial losses, thus dictating the choice of novel conductivity profiles that capture steep wave fluctuations. Overall, the proposed strategy – distinct from its enhanced accuracy – offers a salient annihilation of dispersion, dissipation or anisotropy errors, and so can constitute a useful tool for the solution of complex 3-D electromagnetic problems.

The essence of numerical dispersion in the FDTD method

Numerical dispersion is an undesired non-physical effect inherently present in the FDTD method. Generally, this artificially-created lattice deficiency affects the accurate update of the simulated waves in the computational space by enforcing a strict dependence of phase velocity on frequency (i.e. modal wavelength), propagation direction and grid discretisation. The consequences of dispersion are several and sometimes – along with the problem under study – may become very serious or yet prohibitive for the accomplishment of the analysis. Among them, we can distinguish the cumulative delay or phase errors and the unnatural refraction. According to the former, the inevitable discrepancies from the original speed of light arouse a series of phenomena such as amplification of single-pulse waveforms, generation of vector parasites and mesh anisotropy. So, if a device is based on phase cancelling, even an apparently small error in wave velocity is likely to accumulate to unacceptable levels. Additionally, this sort of error is principally responsible for the dislocation of resonances in the frequency domain, an issue that is proven to be critical in the performance of the second-order Yee scheme at waveguide applications. Conversely, pseudo-refraction is present when the cell shape varies over the lattice namely, in curvilinear, non-orthogonal or unstructured ensembles. Under these circumstances, a wave experiences a diverse numerical speed in different mesh sections. Such a shortcoming corresponds to an inhomogeneous medium which causes refraction to take place. The above remarks demonstrate that dispersion comprises a serious issue in FDTD modeling able to specify its accuracy bounds and if neglected or not effectively suppressed it may easily spoil the entire solution, especially for electrically large structures. As it can not be totally eliminated (after all it is an intrinsic attribute of the discrete state), efforts have focused on its mitigation or, given the suitable conditions, on its compensation. Particularly, every new technique aims at the improvement of the dispersion relation governing plane wave propagation. Initial efforts were directed towards the case of a homogeneous medium and asserted that grid velocity may decrease as the discretisation becomes coarser. However, homogeneous waveforms, by themselves, do not create a complete basis capable of representing all valid field distributions. The general analysis reveals that, for very coarsely-resolved fields, homogeneous waves accept exponential decay, while constraints are established for the propagation speed in the grid. Hence, the use of finer grids could play the role of a definite treatment. Unfortunately, the idea of a larger lattice is not always viable since it implies excessive memory requirements. Bearing in mind that the problems where dispersion becomes more prominent, are already heavily-discretised due to their structural details, it is easy to realise the insufficiency of the above abstraction. Not to mention that after a specific maximum number of cells, the FDTD simulation can not receive further enhancements because of its inherently approximate nature.

The decisive role of numerical dispersion in the development of the Yee algorithm has been the subject of considerable research. Arguably, one of the most efficient and contemporary approaches are the conventional higher-order FDTD techniques [22]-[27] which adopt an advanced tessellation policy that remains in absolute consistency with the specifications pertinent to the modeling of the geometry and the assignment of global field quantities to space-time entities. The principles of the leapfrog integration process are then firmly established by the discrete constitutive equations that guarantee a correct time-advancing without any peculiar unstable results. Owing to the strong relation of higher-order finite-difference schemes to the principles of differential geometry and algebraic topology, especially in curvilinear implementations, our analysis will start by considering a general quantitative framework that delves into their most significant properties. As a matter of fact, the language of differential forms and their discrete counterparts (namely, the cochains) provides an eloquent means for the derivation of dispersionless and stable FDTD simulations.

The differential nature of Maxwell's laws

Despite the fact that the second-order approximation rationale applied to many electromagnetic field problems has

been proven instructive for the extraction of acceptable solutions, their accuracy is sometimes deceptive, since the tenet to regard electric and magnetic fields as plain vectors and functions is essentially misleading. Actually, these quantities must be considered as differential forms i.e. mappings assigning values to oriented manifolds of diverse dimensions. In this manner, we can attain a substantial profit from a design, comprehension and error analysis point of view, whereas our discretisation schemes are more general and consistent.

The theory of differential forms [28]-[41] enables the separation of field equations into topological and metric dependent issues under a unified perspective. Unlike other approaches, the ensuing topological formulae remain completely invariant under different structures or grids thus accepting an exact spatial rendering. Hence, various theoretical constraints (such as divergence-preserving conditions and unisolvence) are inherently fulfilled after discretisation. On the other hand, metric notions have to be enforced only in conjunction with Hodge operators whose primary task is the involvement of constitutive relations in the solution process. In brief, due to differential forms, we accomplish discrete models that inherit the majority of the global attributes of the physical problem and shed light to the interpretation of several rudimentary mechanisms.

Let us assume a general electromagnetic field formulation defined on a (piecewise) smooth oriented and bounded Riemannian manifold M of dimension D in a Euclidean affine space $A(\mathbb{R}^n)$. A differential form Ω^p of order p is a mapping from M into the (D, p)-dimensional space of alternating p-multilinear forms on $\mathbb{R}^n$. In our analysis, the fundamental tool is the exterior derivative d, which maps p-forms into (p+1)-forms. In 3-D problems, d defines the conventional differential operators *grad*, *div* and *curl* for 0-forms through 2-forms, respectively. Alternatively, the exterior derivative may be applied to any differentiable manifold without the need of specifying a certain metric. According to the above, our initial theory can be constructed by using the following concepts: p-forms, Ω^p, which are typically generalised antisymmetric tensors, the exterior derivative $d:\Omega^p \to \Omega^{p+1}$, the Hodge star operator $*:\Omega^p \to \Omega^{D-p}$, required to prescribe scalar quantities, and the exterior product $\wedge:\Omega^p \wedge \Omega^q = \Omega^{p+q}$. Our objective is the development of discrete analogues of these concepts via the satisfaction of the subsequent relations

$$\Omega^p \wedge \Omega^q = (-1)^{pq}\,\Omega^q \wedge \Omega^p\,, \tag{1}$$

$$d(\Omega^p \wedge \Omega^q) = d\Omega^p \wedge \Omega^q + (-1)^p\,\Omega^p \wedge d\Omega^q\,, \tag{2}$$

$$*\Omega^p = \Omega^{D-p}\,, \qquad ** = (-1)^{Dp+1}\,, \tag{3a}$$

$$d^2 = 0\,, \qquad (d^*)^2 = 0\,. \tag{3b}$$

Furthermore, it is important to define two additional objects: (a) the Laplacian on p-forms $\mathrm{L}_p = d_{p-1}d_p^* + d_{p+1}^* d_p$ and (b) the inner product $\left\langle \Omega^p, \Omega^q \right\rangle = \int_M \Omega^p \wedge *\Omega^q$ which will be proven very useful during the establishment of the higher-order non-standard FDTD schemes. In this manner, the hyperbolic system of Maxwell's equations may be expressed as

$$\nabla \times \mathbf{E} = -j\omega\mathbf{B} - \mathbf{J}_M \Rightarrow dE = -j\omega B - J_M\,, \tag{4}$$

$$\nabla \times \mathbf{H} = j\omega\mathbf{D} + \mathbf{J}_E \Rightarrow dH = j\omega D + J_E\,, \tag{5}$$

$$\nabla \cdot \mathbf{B} = 0 \Rightarrow dB = 0\,, \qquad \nabla \cdot \mathbf{D} = \rho \Rightarrow dD = \rho\,. \tag{6}$$

The bold face letters in (4)-(6) indicate the vectorial nature of field quantities, while E and H represent electric and magnetic intensity 1-forms, D and B are the corresponding flux 2-forms, J_E and J_M the electric and magnetic current density 2-forms and ρ the electric charge density 3-form. To complete the description of Maxwell's laws, it is mandatory to link the 1-forms E, H to the 2-forms D, B through the proper $*_\varepsilon$ and $*_\mu$ Hodge operators and the resulting constitutive relations. Consequently, for an arbitrary set of media, we can write that

$$D = *_\varepsilon E\,, \qquad B = *_\mu H\,. \tag{7),(8}$$

Basically, Hodge constituents defy a straightforward way for discretising spaces of differential forms on general meshes sharing attributes of intrinsic duality. The discrete nature of these expressions is confirmed not only from their application as differential operators inside infinitesimal domains, but also from their unperturbed validity in macroscopic regions. They are consequently natural candidates for robust time integrators in the FDTD method. Such a statement, however, requires that the very first stage in the discretisation of a problem should be the punctual discrimination of this special set of relations. Given their initial profile, (4)-(6) can now be rigorously expressed as algebraic linkages between integrated field vectors from which the respective differential forms are derived. Conversely, this kind of distinction to algebraic and differential representations is compatible to the separation of discrete and continuous analogues of physical terms. A very instructive way to realise the importance of the previous remarks is the comprehension of the fundamental difference that distinguishes quantities related to points (i.e. obtained by means of a limit process) from those associated with domains of non-infinitesimal extension (i.e. obtained via integration). Keeping in mind that all approximations, in a numerical technique, are meant to be a function of the latter terms – directly connected to the elementary cells of the discretised meshes – it is reasonable to prefer them as the state variables of our simulation.

Spatial mapping of differential forms via algebraic topology

In this section, we will proceed to the spatial and temporal discretisation of equations (4)-(6) by assigning linear functions of particular lattice elements to the previously defined differential forms. In other words, the transition from the continuous to discrete state postulates the establishment of the suitable correspondence between the physical domain and the FDTD mesh. For this objective, our method will incorporate several topological aspects such as those of a cell complex, a chain and a cochain [35]-[41]. These notions are going to permit the consistent construction of well-posed higher-order schemes as well as prepare the systematic development of reflectionless absorbers for open-boundary problems.

Let us consider a set of affine points spanning over a region in the Euclidean space which is further divided into a set of subdomains composed of adjacent (not overlapping) cells of arbitrary shape and dimension. This set is designated as a cell complex K whose elements – depending on the system's dimensionality – may be vertices (0-cells), edges (1-cells), faces (2-cells) and volumes (3-cells). Presuming a constant orienta-

tion for every c_i^p $(p = 0,1,2,3)$ cell, a p-dimensional chain or simply a p-chain is defined as the linear combination of p-cells in K by means of the following relation

$$\mathbf{c}_p = \sum_i w_i c_i^p, \qquad c_i^p \in K, \tag{9}$$

where coefficients w_i are integers that take the value of 0, 1, or -1 to indicate whether a cell of the complex does not belong to $\mathbf{c}_p$ or is included in it with the default or opposite orientation. It is to be stressed that the space of chains is a vector space over $\mathbb{R}$, since we may easily classify an operation of addition of chains and one of multiplication of a chain by a real number. In a similar manner and given a p-chain $\mathbf{c}_p$, its boundary $\partial^c \mathbf{c}_p$ is a (p-1)-chain that comprises no overlapping cells of lower dimension. The boundary operator ∂^c: $\mathbf{c}_p \rightarrow \mathbf{c}_{p\text{-}1}$ (not to be confused with partial derivative ∂) is a very important element of algebraic topology acting linearly on the space of chains.

It becomes apparent that the theory of chains has a great deal of common abstractions with that of differential forms. In fact, the space of p-forms can be viewed as the dual counterpart of the space of p-dimensional surfaces. Nonetheless, what is the exact relation between the two quantitative tools? To answer this question, we utilise the meaning of cochains which enable the discrete representation of differential forms on the mesh. Assuming, again, an oriented cell complex K and a field F, a function $\mathbf{C}^p$, which appoints an element f^i of F to each cell c_i^p of K, under the notation of $\langle c_i^p, \mathbf{C}^p \rangle = f^i$ is called a p-cochain. Observe that $\mathbf{C}^p$ satisfies

$$\langle \mathbf{c}_p, \mathbf{C}^p \rangle = \langle \sum w_i c_i^p, \mathbf{C}^p \rangle = \sum w_i \langle c_i^p, \mathbf{C}^p \rangle. \tag{10}$$

In essence, the preceding ideas demonstrate the operation of physical fields on domains divided into cell complexes, where the cochain, like a field, associates a value with each cell in an additive way[◊]. Apart from electromagnetic quantities in (4)-(6) that will be described through the dual lattice counterparts of (9) and (10), the principle of exterior derivative d should also be analogously denoted. This is accomplished by defining the coboundary operator, Δ, which transforms a p-cochain $\mathbf{C}^p$ into a (p+1)-cochain $\Delta\mathbf{C}^p$, fulfils the relation

$$\langle \mathbf{c}_{p+1}, \Delta\mathbf{C}^p \rangle \triangleq \langle \partial^c \mathbf{c}_{p+1}, \mathbf{C}^p \rangle \qquad \forall \mathbf{c}_p \in C_p, \tag{11}$$

and provides an exact definition of d. Equation (11) implies that operator Δ associates to each (p+1)-cell the sum of the values that the p-cochain assigns to the p-cells forming the boundary of the (p+1)-cell. In other words, Δ takes a quantity assigned to the boundary of a geometric object and transfers it to the object itself.

The theoretical framework, so far described, achieves an exact discretisation of *div*, and *grad* operators corresponding to the application of ∂^c on 3-, 2- and 1-cells, respectively. Consequently, if we, now, recall the system of Maxwell's equations in (4)-(6) and utilise the concepts of (9)-(11), we obtain

◊ This mapping procedure from the space of p-forms to the space of p-cochains is called the *de Rham map*, while the "inverse" process of associating Ω^p to $\mathbf{C}^p$ is known as the *Whitney map*.

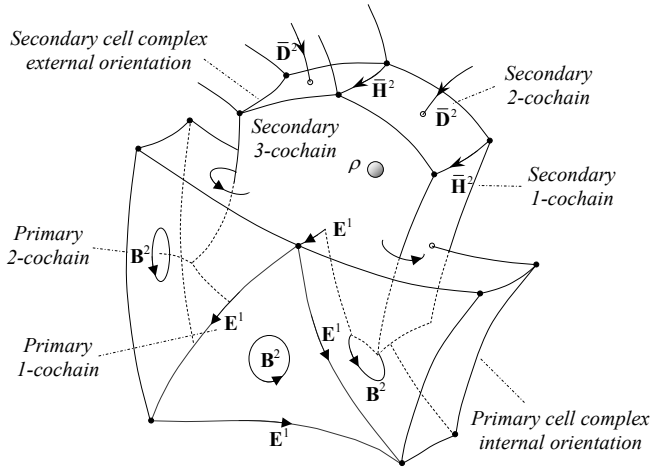

Fig. 1. A generalised curvilinear lattice with its two oriented cell complexes and the locations of field cochains as the discrete counterparts of the corresponding differential forms.

$$\langle \mathbf{c}_2, \Delta\mathbf{E}^1 \rangle = \langle \partial^c \mathbf{c}_2, \mathbf{E}^1 \rangle = -j\omega \langle \mathbf{c}_2, \mathbf{B}^2 \rangle - \langle \mathbf{c}_2, \mathbf{J}_M^2 \rangle, \tag{12}$$

$$\langle \bar{\mathbf{c}}_2, \Delta\mathbf{H}^1 \rangle = \langle \partial^c \bar{\mathbf{c}}_2, \mathbf{H}^1 \rangle = j\omega \langle \bar{\mathbf{c}}_2, \mathbf{D}^2 \rangle + \langle \bar{\mathbf{c}}_2, \mathbf{J}_E^2 \rangle, \tag{13}$$

$$\langle \mathbf{c}_3, \Delta\mathbf{B}^2 \rangle = \langle \partial^c \mathbf{c}_3, \mathbf{B}^2 \rangle = 0, \tag{14a}$$

$$\langle \bar{\mathbf{c}}_3, \Delta\mathbf{D}^2 \rangle = \langle \partial^c \bar{\mathbf{c}}_3, \mathbf{D}^2 \rangle = \langle \bar{\mathbf{c}}_3, \rho \rangle, \tag{14b}$$

where $\mathbf{E}^1$, $\mathbf{H}^1$ are 1-cochains and $\mathbf{B}^2$, $\mathbf{D}^2$ are 2-cochains. The bars over the 2- and 3-chains indicate the two dual (oppositely oriented) cell complexes involved in our calculations whose basic attributes will be analysed in the next section. Equations (12)-(14) give the exact grid counterparts of (4)-(6) and remain unchanged for any mesh with the same structural profile, namely invariant under diverse homeomorphisms.

Duality of oriented cell complexes and Hodge operators

In the previous section, we encountered the idea of dual cell complexes which, also, characterises the fundamental structure of the FDTD algorithm. Duality in lattice construction is strongly related to the issue of oriented forms. Actually, one can discern two kinds of orientations for 3-D discretisations (Fig. 1); the externally-oriented regime (external or outer orientation) that circulates the object and involves additional dimensions and the internal one (internal or inner orientation) specifying a certain direction along the object without increasing its dimensionality. Obviously, from a geometrical point of view, there are two types of forms associated with these orientations. The primary forms which are internally-oriented and the secondary forms sharing an outer orientation. It is stressed that this designation is not unique, since in [37], the terms ordinary and twisted forms are, respectively, utilised.

As anticipated, the meaning of orientation should be applicable to cell complexes, establishing thus the duality premise in the discrete state. Therefore, a primary cell complex, K, consists of internally-oriented cells linked to cochains that represent primary forms, while the secondary cell complex, $\bar{K}$, contains cells with external orientation associated with cochains that are secondary forms. Then, for every p-cell of the primary complex there exists a corresponding (D-p)-cell of the dual one. This assignment consists in the fact that a primary p-

cell contains or crosses a dual (*D*-*p*)-cell, as shown in Fig. 1. To conduct an one-to-one mapping between electromagnetic fields and the prior classification, we denote the electric field, **E**, as a primary 1-form (internally-oriented lines), the magnetic field, $\bar{\mathbf{H}}$, as a secondary 1-form (externally-oriented lines), the magnetic flux, **B**, as a primary 2-form (internally-oriented surface), the electric flux, $\bar{\mathbf{D}}$, as a secondary 2-form (externally-oriented surface) and the electric charge density, ρ, as a secondary 3-form (externally-oriented volume).

Having determined the dual character of the lattice, our analysis proceeds to the action of the discrete Hodge operators which must relate the primary to the secondary forms and incorporate the properties of the media occupying the computational domain. Since, the continuous operators attain a linear assignment of *p*-forms to (*D*-*p*)-forms, one may write

$$[*_\varepsilon]: K \to \bar{K} \qquad \left\langle \bar{\mathbf{c}}_2, \bar{\mathbf{D}}^2 \right\rangle = [*_\varepsilon] \left\langle \mathbf{c}_1, \mathbf{E}^1 \right\rangle, \tag{15}$$

$$[*_\mu]: \bar{K} \to K \qquad \left\langle \mathbf{c}_2, \mathbf{B}^2 \right\rangle = [*_\mu] \left\langle \bar{\mathbf{c}}_1, \mathbf{H}^1 \right\rangle, \tag{16}$$

in which $[*_\varepsilon]$ and $[*_\mu]$ are square and sparse matrices (tensors). The most striking difference between the discretised constitutive equations (15)-(16) and the topological entities of (12)-(14) is the metric nature of the former. This implies that they require the use of lengths, surfaces, volumes etc, exhibiting so a completely approximating profile as opposed to their physical counterparts. This is exactly where numerical methods should be applied for the best accuracy. Unfortunately, second-order Yee schemes have been found insufficient for several categories of complex 3-D problems, such as scattering or waveguide applications. In fact, this crucial observation has been the essential motive for the formulation of our higher-order non-standard FDTD methodology, especially in curvilinear coordinates, where discrepancies are usually so serious that prohibit the entire simulation.

The higher-order non-standard FDTD methodology

The basic features of the proposed 3-D strategy are the new higher-order (HO) non-standard concepts that overwhelm all conventional formulae. Their superior profile is further enhanced by the low wavelength-to-stencil ratio and the reduced number of iterations. In fact, non-standard differencing [42]-[45] is an extremely promising theoretical framework for the accurate analysis of complicated problems in electromagnetics and the approximation of 1- and 2-cochains in (15) and (16). We start by introducing three spatial operators which correspond to *u*,*v*,*w* axes of a general coordinate system (*u*,*v*,*w*) – defined as $\mathbf{S}_u[.]$, $\mathbf{S}_v[.]$, $\mathbf{S}_w[.]$ – and one temporal operator $\mathbf{T}[.]$. These are given by

$$\begin{aligned}\mathbf{S}_u\left[f\big|_{u,v,w}^t\right] &= b_1 \mathbf{P}_{\delta u}^u\left[f\big|_{u,v,w}^t\right] + b_2 \mathbf{P}_{3\delta u}^u\left[f\big|_{u,v,w}^t\right] \\ &\quad + b_3\left(f\big|_{u-\delta u/2,v,w}^t - f\big|_{u-3\delta u/2,v,w}^t\right)/\delta u,\end{aligned} \tag{17}$$

$$\begin{aligned}\mathbf{T}\left[f\big|_{u,v,w}^t\right] &= \left(f\big|_{u,v,w}^{t+\delta t/2} - f\big|_{u,v,w}^{t-\delta t/2}\right)/c_T(k\delta t) \\ &\quad - 2b_3 \sum_{\tau=3\ (odd)}^{T_s} \frac{1}{\tau!}\left[\frac{c_T(k\delta t)}{2}\right]^{\tau-1} \frac{\partial^\tau f}{\partial t^\tau}\bigg|_{u,v,w}^n,\end{aligned} \tag{18}$$

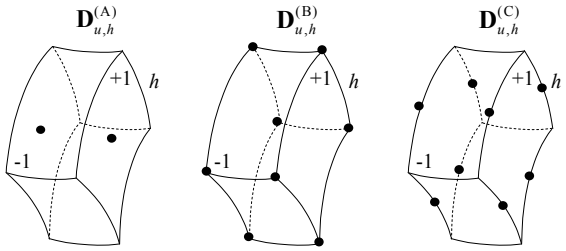

Fig. 2. Graphical depiction of the sampling points for the three difference operators in a general cell complex. The +1 and -1 numbers at the faces indicate the sign of summation for the values of the approximated function.

with $\mathbf{S}_v[.]$ and $\mathbf{S}_w[.]$ designed in a similar manner to compute spatial derivatives with respect to *v* and *w*, respectively. The summation parameter τ, in (18), is running from 3 to T_s, where T_s is an odd predefined upper limit that controls the order of time derivative approximation according to the accuracy level. Let us, now, focus on the HO non-standard schemes and explain their structure. By setting $b_1 = 9/8$, $b_2 = -1/24$, $b_3 = 0$, we get the basic member of the class, while for $b_1 = 11/12$, $b_2 = 1/24$, $b_3 = 1/24$ the second counterpart is extracted, with δu, δv, δw its spatial and δt its temporal increments. In (17), $\mathbf{P}_h^u[.]$ for $h = \delta u, 3\delta u$, is the 3-D non-standard operator, defined as

$$\begin{aligned}\mathbf{P}_h^u\left[f\big|_{u,v,w}^t\right] \equiv \frac{1}{c_S(kh)}\Big\{ & p_{\mathrm{A}}\mathbf{D}_{u,h}^{(\mathrm{A})}\left[f\big|_{u,v,w}^t\right] \\ & + p_{\mathrm{B}}\mathbf{D}_{u,h}^{(\mathrm{B})}\left[f\big|_{u,v,w}^t\right] + p_{\mathrm{C}}\mathbf{D}_{u,h}^{(\mathrm{C})}\left[f\big|_{u,v,w}^t\right]\Big\}.\end{aligned} \tag{19}$$

Correction functions $c_S(kh)$, $c_T(k\Delta t)$ are selected to minimise the lattice errors and guarantee the smooth transition from the continuous physical space to the discrete confined domain. Investigating $c_S(kh)$, mathematical analysis reveals that *kh* values should be chosen in order $\mathbf{P}_h^u[e^{jku}]/\partial_u e^{jku} \to 1$. It is stressed, that the second-order FDTD technique can not satisfy this important requirement in curvilinear applications inducing thus, severe instabilities. To select an acceptable *kh* for several wavenumbers *k*, the Fourier transform of the already computed transient electric (magnetic) components, at prefixed mesh locations, is used. After their frequency range is acquired, we use the spectrum's maximum value for the specification of the optimal argument. The process, which does not affect the total overhead, takes place at every time-step, whereas its accuracy increases as the number of the preset points becomes larger regardless the problem's geometry, incident angles or frequencies and time intervals. It is clear, that the same holds for $c_T(k\Delta t)$, especially from a convergence point of view.

Through these notions, a possible (but not unique) choice for the correction functions [44] could be

$$c_T(\delta t) = \frac{5}{\delta t}\sin\left(\frac{\delta t}{4}\right) + \frac{10}{(\delta t)^2}\cos^2\left(\frac{\delta t}{8}\right). \tag{20}$$

On the other hand, operators $\mathbf{D}_{u,h}^{(i)}[.]$ for *i* = A,B,C, in (19), lead to a set of formulae which offer a systematic cochain interconnection. Establishing the general curvilinear geometry of Fig. 2, one derives

$$\mathbf{D}_{u,h}^{(\mathrm{A})}\left[f\big|_{u,v,w}^t\right] = f\big|_{h/2,0,0}^t - f\big|_{-h/2,0,0}^t, \tag{21}$$

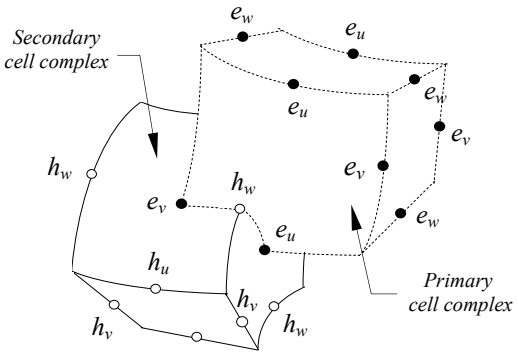

Fig. 3. A non-orthogonal FDTD lattice comprising two dual cell complexes.

$$\mathbf{D}^{(\mathrm{B})}_{u,h}\left[f\big|^{t}_{u,v,w}\right]=\frac{1}{4}\begin{pmatrix} f\big|^{t}_{h/2,\delta v,\delta w}+f\big|^{t}_{h/2,\delta v,-\delta w}+f\big|^{t}_{h/2,-\delta v,\delta w} \\ +f\big|^{t}_{h/2,-\delta v,-\delta w}-f\big|^{t}_{-h/2,\delta v,\delta w}-f\big|^{t}_{-h/2,\delta v,-\delta w} \\ -f\big|^{t}_{-h/2,-\delta v,\delta w}-f\big|^{t}_{-h/2,-\delta v,-\delta w} \end{pmatrix}, \quad (22)$$

$$\mathbf{D}^{(\mathrm{C})}_{u,h}\left[f\big|^{t}_{u,v,w}\right]=\frac{1}{4}\begin{pmatrix} f\big|^{t}_{h/2,\delta v,0}+f\big|^{t}_{h/2,-\delta v,0}+f\big|^{t}_{h/2,0,\delta w} \\ +f\big|^{t}_{h/2,0,-\delta w}-f\big|^{t}_{-h/2,\delta v,0}-f\big|^{t}_{-h/2,-\delta v,0} \\ -f\big|^{t}_{-h/2,0,\delta w}-f\big|^{t}_{-h/2,0,-\delta w} \end{pmatrix}, \quad (23)$$

where only the respective lattice increments towards the u,v,w are indicated (i.e. the subscript $h/2,-\delta v,0$ means $u+h/2,v-\delta v,w$). Of particular importance, also, are the p_i parameters, since they evade the ill-posedness of the conventional second-order PML arrangements and certify algorithmic consistency. Therefore,

$$p_{\mathrm{A}}=q+\eta(1-q)/3\ , \quad (24a)$$

$$p_{\mathrm{B}}=\eta(1-q)/3\ , \quad (24b)$$

$$p_{\mathrm{C}}=1-q-2\eta(1-q)/3\ , \quad (24c)$$

with

$$\eta=\frac{qQ_{\mathrm{A}}+(1-q)Q_{\mathrm{B}}-(\cos k-1)}{(q-1)(Q_{\mathrm{A}}+Q_{\mathrm{B}}-2Q_{\mathrm{C}})}, \quad (25a)$$

$$q=\frac{\cos k_u\cos k_v\cos k_w-\cos k}{1+\cos k_u\cos k_v\cos k_w-\cos k_u-\cos k_v-\cos k_w}\ , \quad (25b)$$

while coefficients Q_i are computed through the components of wavenumber $\mathbf{k}$, as

$$Q_{\mathrm{A}}=\cos k_u+\cos k_v+\cos k_w-3\ , \quad (26)$$

$$Q_{\mathrm{B}}=\cos k_u\cos k_v\cos k_w-1\ , \quad (27)$$

$$Q_{\mathrm{C}}=0.5(\cos k_u\cos k_v+\cos k_u\cos k_w+\cos k_v\cos k_w-3)\ . \quad (28)$$

Notice that as soon as the space-time domain quantities of the problem, under investigation, are properly discerned and the correct discretisation strategy has been chosen, the type of time integration is uniquely determined. This is opposed to other existing approaches which conduct two separate actions for the solution of a problem i.e. they first discretise the domain in space and then form the set of differential equations that are approximated in the time variable through one of the many techniques developed for numerical update. The topological interpretation of the proposed method has an additional advantage; it reveals the pitfalls of the classical outlook, which if disregarded, yield an unstable algorithm that does not adhere to the physics of the problem, an instance more frequently encountered in curvilinear implementations.

Modeling the curvilinear div-curl formulation

Consider a 3-D domain described by an arbitrary ($u = i\delta u$, $v = j\delta v$, $w = k\delta w$) system and discretised into uniform cells which form two dual cell complexes. From the Figure 3, we observe that covariant, h_m, and contravariant, h^l, components ($l,m = u,v,w$) of magnetic vectors, $\mathbf{H}$, are located at secondary edges remaining so in complete interleaving with e_m and e^l quantities of electric vectors, E**,** placed at primary edge centers. The new scheme hosts the idea of fluxes for the fields across the faces defined by $f^{(l)} = g^{1/2}f^l$ ($f = e,h$), with g_{lm} the coordinate metrics. Representation of f_m with f^l is achieved via the chain rules $f_m = g_{ml}f^l$ and $f^l = g^{lm}f_m$. Next, we introduce the linear operator $\mathbf{Q}^{(l)}$ such that $f^{(l)} = \mathbf{Q}^{(l)}[f_m]$, which uses the local components f_m and the neighboring ones f_{m+1}, f_{m+2} ($m+1$, $m+2$ denote a consecutive cyclic permutation of u,v,w), multiplied by the discrete metric terms. For instance, the $\mathbf{Q}^{(u)}[h_u]$ becomes

$$\begin{aligned}\mathbf{Q}^{(u)}\left[h_u\big|^{n+1/2}_{i-1/2,j,k}\right]=&\,s^{uu}_{i-1/2,j,k}\,h_u\big|^{n+1/2}_{i-1/2,j,k}+\frac{1}{4}\Big[s^{uv}_{i,j,k}(h_v\big|^{n+1/2}_{i,j-1/2,k}+h_v\big|^{n+1/2}_{i,j+1/2,k}) \\ &+s^{uv}_{i-1,j,k}(h_v\big|^{n+1/2}_{i-1,j-1/2,k}+h_v\big|^{n+1/2}_{i-1,j+1/2,k})+s^{uw}_{i,j,k}(h_w\big|^{n+1/2}_{i,j,k-1/2}+h_w\big|^{n+1/2}_{i,j,k+1/2}) \\ &+s^{uw}_{i-1,j,k}(h_w\big|^{n+1/2}_{i-1,j,k-1/2}+h_w\big|^{n+1/2}_{i-1,j,k+1/2})\Big],\end{aligned} \quad (29)$$

where $s^{lm} = g^{1/2}g^{lm}$. Flux analysis is indeed very instructive as it circumvents all complicated projections for primary and secondary fields (cochains). By substituting operators (17), (18) into Maxwell's laws (12)-(15), it is derived that

$$\begin{aligned}(\mathbf{I}+\tfrac{1}{2}\mathbf{Y}_t)\mathbf{E}^{n+1}_{cv}=&\,(\mathbf{I}-\tfrac{1}{2}\mathbf{Y}_t)\mathbf{E}^{n}_{cv}-c_T(k\delta t)\varepsilon^{-1}\mathbf{J}^{n+1/2}_{E,cv} \\ &+\mathbf{G}^{H}\mathbf{S}[\mathbf{H}^{n+1/2}_{cv}]+\mathbf{T}^{n+1/2}_{E}\end{aligned}, \quad (30)$$

$$\begin{aligned}(\mathbf{I}+\tfrac{1}{2}\mathbf{R}_t)\mathbf{H}^{n+1/2}_{cv}=&\,(\mathbf{I}-\tfrac{1}{2}\mathbf{R}_t)\mathbf{H}^{n-1/2}_{cv}-c_T(k\delta t)\mu^{-1}\mathbf{J}^{n}_{M,cv} \\ &-\mathbf{G}^{E}\mathbf{S}[\mathbf{E}^{n}_{cv}]+\mathbf{T}^{n}_{H}\end{aligned}, \quad (31)$$

in which cv are the covariant components, $\mathbf{Y}_t$, $\mathbf{R}_t$ the constitutive matrices and $\mathbf{G}_{\mathrm{F}}$, $\mathbf{T}_{\mathrm{F}}$ (for $\mathbf{F} = \mathbf{E}$, $\mathbf{H}$) metric tensors and matrices of HO time derivatives, respectively. Notice that all quantities in (30), (31) retain their algebraic structure according to the theory of chains and cochains. More specifically,

$$\mathbf{E}^{n+1}_{cv}=\left\langle \mathbf{c}_1,\mathbf{E}^1\right\rangle^{n+1}_{cv} \quad \text{and} \quad \mathbf{H}^{n+1}_{cv}=\left\langle \overline{\mathbf{c}}_1,\overline{\mathbf{H}}^1\right\rangle^{n+1/2}_{cv}. \quad (32)$$

For the widened spatial stencils near absorbing or perfectly conducting walls, a broad classification of compact self-adaptive schemes is developed.

$$\sum\nolimits_{s=-1}^{1}(a_{\mathrm{A}}\,f_u\big|^{n}_{i+s}+a_{\mathrm{B}}\,f_u\big|^{n}_{i}+a_{\mathrm{C}}\,f_u\big|^{n}_{i-s})=0\ , \quad (33)$$

where a_{A}, a_{B}, a_{C} are pre-selected real numbers. It is apparent that the time-marching procedure for the update of $\mathbf{E}$ and $\mathbf{H}$ fields in (30), (31), should be selected in order to avoid late-time instabilities or slow convergence. Among the existing

techniques, we can distinguish the one described in [22] and the Runge-Kutta integrators [24]. The former converts the HO order time derivatives into spatial ones by the consecutive use of Maxwell's equations, while the latter staggers the variables in space but not in time via an implicit system of equations. Although efficient up to the fourth-order, these schemes become impractically complicated at HO non-standard cases and inhibit the entire simulation. Therefore, to avoid a complicated time marching, we employ a generalised leapfrog formulation, suitably built to account for lossy dielectrics as well. Integrating field components in a constant regime, the technique divides each time-step to a number of stages equal to the order of approximation and requires resources that hardly influence the total burden. For instance, the update of **H** is given by

$$\boldsymbol{\Theta}_{\mathrm{A}} = (\delta t/\varepsilon)\nabla\times\mathbf{H}^{n+1/2}, \qquad \boldsymbol{\Theta}_{\mathrm{B}} = -(\delta t/\mu)\nabla\times\boldsymbol{\Theta}_{\mathrm{A}}, \quad (34a)$$

$$\boldsymbol{\Theta}_{\mathrm{C}} = (\delta t/\varepsilon)\nabla\times\boldsymbol{\Theta}_{\mathrm{B}}, \qquad \mathbf{E}^{n+1} = \mathbf{E}^{n} + \boldsymbol{\Theta}_{\mathrm{A}} + \boldsymbol{\Theta}_{\mathrm{C}}/24. \quad (34b)$$

The major issue of stability for the HO non-standard algorithm is attained by the non-orthogonal Courant criterion

$$c\delta t \le \frac{3}{\pi}\sin^{-1}(0.7)\left(\sum_{l=u}^{w}\sum_{m=u}^{w}\frac{g^{lm}}{\delta l\,\delta m}\right)^{-1/2}. \quad (35)$$

Finally, to demonstrate the efficiency of our technique, we compare its dispersion relation with that of the Yee scheme (c' the numerical velocity, $\beta = 2\pi/(k\delta w)$ and θ the incident angle)

$$\left(\frac{c}{c'}\right)^{Yee} \cong 1-\frac{\pi^2}{\beta^2}\left[\frac{1}{8}+\frac{1}{24}\cos(4\theta)\right], \quad (36a)$$

$$\left(\frac{c}{c'}\right)^{nst} \cong 1-\frac{5\pi^7}{670\beta^7}\left[\frac{1}{19}+12\cos(4\theta)\right], \quad (36b)$$

to attain the remarkable reduction of five orders of magnitude. This implies that the proposed topological strategy diminishes grid defects and annihilates the undesired curvilinear dispersion mechanisms.

Convergent treatment of complex material interfaces

The effects of staircasing and the lack of properly enforced jump-conditions on both sides of arbitrarily-embedded general material interfaces have notable consequences on the stability of the FDTD method. In fact, for cases where a field component is discontinuous along a 3-D curvilinear grid line, the Yee scheme exhibits loss of global convergence. To overcome this drawback, a HO convergent formulation is developed. The technique, unlike other approaches, modifies the stencils around media interfaces to correctly represent their physical location and enforce the proper continuity conditions.

Assume the curvilinear material boundary of Fig. 4, with $\hat{\mathbf{n}} = (\hat{n}_u, \hat{n}_v, \hat{n}_w)^{\mathrm{T}}$ a normal unit vector. Connecting $\mathbf{E}^{mat}$, $\mathbf{H}^{mat}$ in the different materials, ε^{mat} and μ^{mat} (mat = A,B) by the suitable tangential/normal continuity conditions, we use covariant components and correct the problematic $\partial_w h_u$ at the interface as

$$\partial_w h_u\big|^{n+1/2}_{i,k,j} = 2(2\beta^{\mathrm{B}}_{i,j,k}+1)^{-1}(h_u\big|^{n+1/2}_{i+1/2,k,j} - h_u^{\mathrm{B},\,n+1/2})/\delta u, \quad (37a)$$

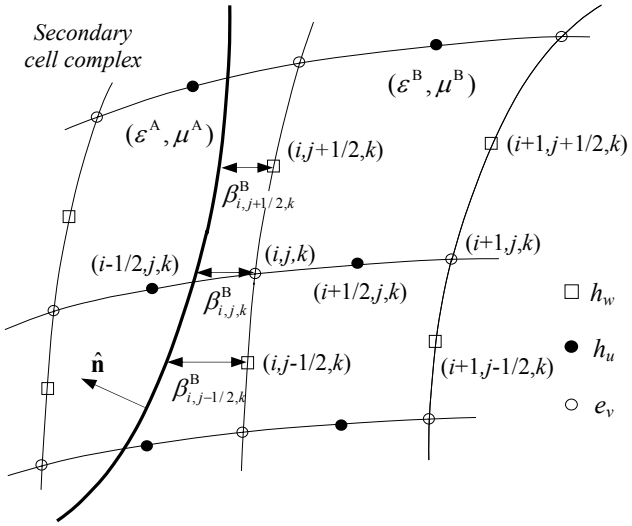

Fig. 4. Treatment of an arbitrary-aligned media interface in a curvilinear mesh.

with $$\beta^{\mathrm{A}}_{i,j,k} = 0.5 - \beta^{\mathrm{B}}_{i,j,k}. \quad (37b)$$

The material term in (37) receives the following calculation

$$\frac{h_u^{\mathrm{B},\,n+1/2} - h_u^{\mathrm{A},\,n+1/2}}{\hat{n}_u(\mu^{\mathrm{A}}-\mu^{\mathrm{B}})} = \frac{\hat{n}_u h_u^{\mathrm{A},\,n+1/2} + \hat{n}_v h_v^{\mathrm{A},\,n+1/2} + \hat{n}_w h_w^{\mathrm{B},\,n+1/2}}{\mu^{\mathrm{A}}\hat{n}_w^2 + \mu^{\mathrm{B}}\hat{n}_u^2 + \mu^{\mathrm{B}}\hat{n}_v^2}, \quad (38)$$

where the three transitional variables in the nominator of (38) are recovered directly by extrapolation. So,

$$h_u^{\mathrm{A},\,n+1/2} = (1+\beta^{\mathrm{A}}_{i,j,k})\,h_u\big|^{n+1/2}_{i-1/2,j,k} + \beta^{\mathrm{A}}_{i,j,k}\,h_u\big|^{n+1/2}_{i-3/2,j,k}, \quad (39a)$$

$$h_w^{\mathrm{B},\,n+1/2} = \tfrac{1}{2}(\tilde{h}_w\big|^{n+1/2}_{i,j+1/2,k} + \tilde{h}_w\big|^{n+1/2}_{i,j-1/2,k}), \quad (39b)$$

$$\begin{aligned} h_v^{\mathrm{A},\,n+1/2} = \frac{1}{4}(&\tilde{h}_v\big|^{n+1/2}_{i,j-1/2,k-1/2} + \tilde{h}_v\big|^{n+1/2}_{i,j+1/2,k-1/2} \\ &+ \tilde{h}_v\big|^{n+1/2}_{i,j+1/2,k+1/2} + \tilde{h}_v\big|^{n+1/2}_{i,j-1/2,k+1/2}), \end{aligned} \quad (39b)$$

with analogous expressions holding for e components. Evaluation of the tilded variables in (39) gives

$$\begin{aligned} \tilde{h}_w\big|^{n+1/2}_{i,j\pm1/2,k} &= h_w\big|^{n+1/2}_{i,j\pm1/2,k} \\ &+ \beta^{\mathrm{B}}_{i,j\pm1/2,k}(h_w\big|^{n+1/2}_{i,j\pm1/2,k} - h_w\big|^{n+1/2}_{i+1,j\pm1/2,k}), \end{aligned} \quad (40a)$$

$$\begin{aligned} \tilde{h}_v\big|^{n+1/2}_{i,j\pm1/2,k\pm1/2} &= h_v\big|^{n+1/2}_{i-1/2,j\pm1/2,k\pm1/2} \\ &+ \beta^{\mathrm{A}}_{i,j\pm1/2,k\pm1/2}(h_v\big|^{n+1/2}_{i-1/2,j\pm1/2,k\pm1/2} - h_v\big|^{n+1/2}_{i-3/2,j\pm1/2,k\pm1/2}). \end{aligned} \quad (40b)$$

The implementation of (37)-(40) involves a predictor-corrector scheme in which the HO non-standard FDTD algorithm, serving as the predictor stage, is used to solve Maxwell's equations in the entire domain, while a corrector stage modifies the solutions locally via the above technique. The slightly increased mathematical complexity is compensated by the impressive accuracy at no additional computational cost and the efficient handling of internal curvilinear interfaces.

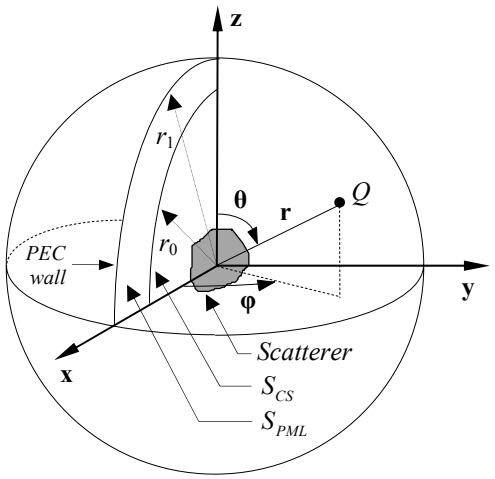

Fig. 5. The 3-D geometry of space S in spherical coordinates.

Construction of dispersionless curvilinear PMLs

The development of the enhanced unsplit-field PMLs in curvilinear coordinates stems from the decomposition of a 3-D space, S, into two regions such that $S = S_{CS} \cup S_{PML}$, where S_{CS} refers to the computational domain and S_{PML} is the area occupied by the PML. Essential in our formulation, is the extension of the stretched-coordinate technique to the HO non-standard models. Establishing the principles of our algorithm, we introduce the following steps:

- Postulation of the field profile in the layer via stretched coordinate metrics.
- Development of the essential equations whose solutions exhibit the required attenuation rate.
- Manifestation of the resulting expressions in the format of HO time-dependent laws.
- Deduction of the constitutive relations in S_{PML} to completely identify the absorber.

Now, let us concentrate, without loss of generality, on spherical coordinates (r,θ,φ) where highly dispersive non-physical reflections generate bands of transmitted modes growing spatially instead of being damped in the layer. Hence, simulations exhibit a totally ill-posed performance even under small perturbations. For our analysis, we examine an inhomogeneous, isotropic and loseless dielectric medium, described in the frequency domain by

$$j\omega\varepsilon\mathbf{E}' = \nabla'\times\mathbf{H}', \qquad \nabla'\cdot(\varepsilon\mathbf{E}') = 0\,, \tag{41a}$$

$$-j\omega\mu\mathbf{H}' = \nabla'\times\mathbf{E}', \qquad \nabla'\cdot(\mu\mathbf{H}') = 0\,. \tag{41b}$$

Here, S_{CS} is a sphere of radius r_0, and S_{PML} the area to be terminated up to a radius r_1 by a perfectly electric wall, as shown in Fig. 5. The optimised PML, is built through the decent scaling between the independent (primed) and dependent variables in (41) which preserve the original field variation in S_{CS} and launch the proper coordinate stretching in S_{PML}. This procedure may be viewed as a mapping of the homogeneous isotropic dielectric to an inhomogeneous uniaxial one. So,

$$\mathbf{F}' = \begin{cases} \mathbf{F}, \text{ for } \mathbf{r}' \in S_{CS} \\ diag\{\zeta_r, \xi_r^{-1}, \xi_r^{-1}\}\mathbf{F}, \text{ for } \mathbf{r}' \in S_{PML} \end{cases}, \tag{42}$$

with $\mathbf{r}' = diag\{\xi_r,1,1\}$, $\mathbf{r} = (r,\theta,\varphi)^{\mathrm{T}}$ and $\mathbf{F} = \mathbf{E},\mathbf{H}$. Application of (42) to the equations of (41) yields

$$j\omega\varepsilon\Xi\cdot\mathbf{E} = \nabla\times\mathbf{H}\,, \qquad -j\omega\mu\Xi\cdot\mathbf{H} = \nabla\times\mathbf{E}\,, \tag{43}$$

where the material tensor $\Xi = diag\{\xi_r^2\zeta_r, \zeta_r^{-1}, \zeta_r^{-1}\}$ for a homogeneous dielectric background with constant constitutive parameters. Gauss law for the **E** and **H** field yields

$$\nabla\cdot(\varepsilon\Xi\cdot\mathbf{E}) = 0\,, \qquad \nabla\cdot(\varepsilon\Xi\cdot\mathbf{E}) = 0\,. \tag{44}$$

Equations (43), (44) compose a causal and strongly well-posed hyperbolic system which permits the physical realisation of the unsplit PML concept. In the above

$$\zeta_r(r,\omega) = \left[1+\frac{\sigma_r(r)}{j\omega}\right]^{-1}, \tag{45a}$$

$$\xi_r(r,\omega) = 1+\frac{\sigma_r'(r)}{j\omega}, \tag{45b}$$

for $$\sigma_r(r) = \sigma_r^{\max}[(r-r_0)/\delta]^{m_d}\,; \qquad m_d \geq 0\,, \tag{45c}$$

$$\sigma_r'(r) = r^{-1}\int_{r_0}^{r}\sigma_r(s)ds\,, \tag{45d}$$

with S_{PML} restricted to a sphere of radius $r_0 + \delta$ and δ the layer's depth. Concentrating on Ampere's law in (41) and after the substitution of (45), we obtain

$$\mathbf{T}[B_r] + \sigma_r'(r)B_r = g_\varphi\mathbf{S}_\varphi[E_\theta] - g_\theta\mathbf{S}_\theta[E_\varphi]\,, \tag{46a}$$

with $$\mathbf{T}[B_r] + \sigma_r(r)B_r = \mu\mathbf{T}[H_r] + \mu\sigma_r'(r)H_r\,;$$

$$\mathbf{T}[B_\theta] = g_r\mathbf{S}_r[E_\varphi] - g_\varphi\mathbf{S}_\varphi[E_r]\,, \tag{46b}$$

with $$\mathbf{T}[B_\theta] = \mu\mathbf{T}[H_\theta] + \mu\sigma_r(r)B_\theta\,;$$

$$\mathbf{T}[B_\varphi] = g_\theta\mathbf{S}_\theta[E_r] - g_r\mathbf{S}_r[E_\theta]\,, \tag{46c}$$

with $$\mathbf{T}[B_\varphi] = \mu\mathbf{T}[H_\varphi] + \mu\sigma_r(r)H_\varphi\,,$$

in which $B_r = \mu\xi_r\zeta_r H_r$ and g_m $(m = r,\theta,\varphi)$ the spherical system metrics. Apart from the previous merits, the proposed strategy assigns a key characteristic to HO PMLs; the ability to introduce supplementary attenuation terms along more directions in the layer which entail a considerable suppression of the strenuous anisotropy discrepancies, especially in multi-frequency environments with many scattering objects.

Numerical verification

The merits of the HO non-standard FDTD-PML method are validated via an indicative set of 3-D curvilinear problems. In the first example, we compare the global error induced by second-order split-field and our HO Maxwellian PML arrangements in spherical coordinates. The dielectric scatterer ($\varepsilon = 4.3\varepsilon_0$), of radius $r_s = 0.5\lambda$, is located at the centre of the origin and excited by $E(t) = 17 - 11\cos\omega_1 t - 8\cos\omega_2 t + 2\cos\omega_3 t$ with $\omega_k = 2\pi k/T$ $(k = 1,2,3)$ and $t \in [0, T = 10^{-9}]$. As deduced from the results of Fig. 6, the proposed absorbers are far more superior to the common ones since they achieve their objective with a sufficiently smaller amount of layers.

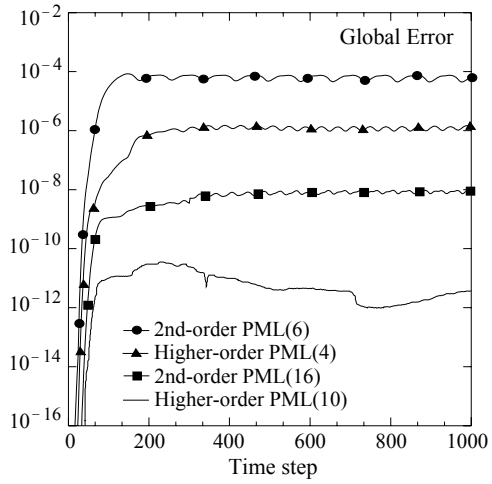

Fig. 6. Global error versus time steps for various second-order and HO PMLs.

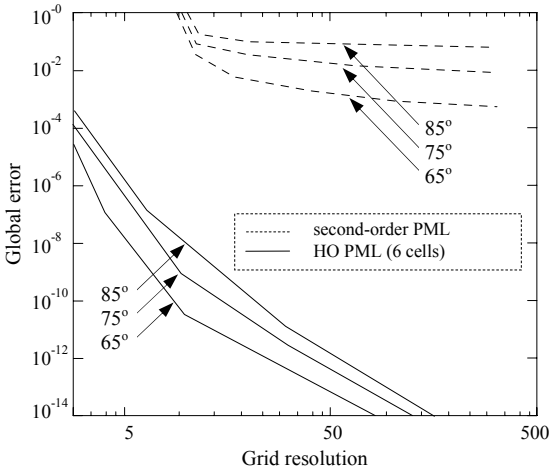

Fig. 7. Convergence rate of global error vs grid resolution for a second-order and a HO non-standard PML at various angles of impingement.

To realise the influence of the grid size on computational resources, we consider a spherical domain S_{CS} = 11×25×38, with a PEC scatterer of r_s = 0.8 m. Given that the radius of S_{CS} is r_0 = 1.2 m, the rest of the FDTD details are δr = 0.109 m, $\delta\theta$ = 0.1256 rad, $\delta\varphi$ = 0.1653 rad and δt = 0.2097 nsec. For the excitation of the structure, we use the steeper Ricker wavelet,

$$P(t) = \gamma\sqrt{P_0/2}\,\frac{d}{dt}e^{-[(t-t_0)/\gamma]^2}h(t)\,, \qquad (47)$$

placed one cell from the PML, with γ = 0.4391 μs, t_0 = 1.5 μs and $h(t)$ the Heaviside pulse. Fig. 7 gives the convergence rate of the global error versus grid resolution, $\delta r/\lambda_{\min}$, for different angles (even near-grazing ones) of wave impingement on the normal to the vacuum-PML interface. For comparison, we choose a second-order PML (δ =10 cells), also imposed one cell from the source. Results present that such a short distance is not enough for the ordinary absorber, since its error is very high and does not converge. Observe that when $\delta r/\lambda_{\min}$ has a low value, e.g. 1/5, this PML has a global error of 10^0 namely, it reflects all outgoing waves. In opposition, its HO non-standard counterpart converges very fast, regardless of its small depth, yielding a striking set of reflection errors as well.

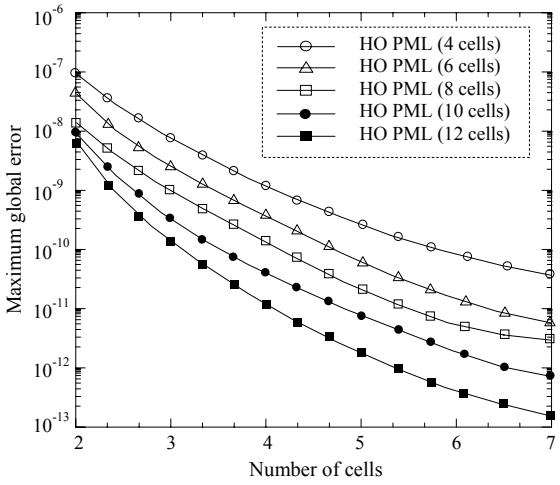

Fig. 8. Maximum global error vs distance from two lossy dielectric spheres induced by different HO non-standard PMLs.

Finally, a set of two lossy dielectric spheres, which are not co-centric, is investigated. The larger sphere ($\varepsilon_1 = 2.3\varepsilon_0$, r_{s1} = 0.7 m, σ_1 = 0.002 S/m) contains the smaller one ($\varepsilon_2 = 5.2\varepsilon_0$, r_{s2} = 0.2 m, σ_2 = 0.75 S/m whose centre is set 0.4 m away from the origin and more specifically at point (0.4,π/2,0). The domain is discretised in 14×29×41 cells with δr = 0.16 m, $\delta\theta$ = 0.1083 rad, $\delta\varphi$ = 0.1532 rad and δt = 0.1547 nsec, and excited by a plane wave. The interesting issue here, is that the boundary of the two objects does not coincide with any of the grid axes making thus, the modeling of the small scatterer via the simple FDTD algorithm, absolutely unfeasible. The chief reason of this shortcoming is the violation of the continuity conditions for the field components at the above boundary, which in its turn induces serious dispersion errors. In Fig. 8, the maximum global error versus distance from the scatterers, for various HO PMLs, is presented. Results are indeed very good and exhibit a smooth evolution for reasonable values of δ.

Conclusions

We have presented a HO non-standard FDTD-PML strategy for the efficient and precise analysis of 3-D electromagnetic problems in general non-orthogonal coordinates. Founded on the principles of differential forms and the theory of algebraic topology, the novel method starts from an elegant way of factorising Maxwell's equations and proceeds to the establishment of a linearly independent covariant/contravariant regime enabling thus, the consistent modeling of the div-curl problem. Moreover, HO concepts assure the philosophy of the oriented dual grids and postulate a concise outline for the analysis of the discrete vector fields. As a consequence, a class of accurate dispersionless HO PMLs operators, ideal for curvilinear mapping, is designed. Numerical results, addressing several demanding applications, prove that the proposed algorithm eliminates the intricacy of fictitious waves, conducts remarkably accurate simulations and achieves significant savings of total computational requirements. Considering the constant needs for advanced numerical models and the continuous studies in the evolution of numerical absorption, it is expected that the theory of HO non-standard forms will constitute a functional tool for the treatment of demanding applications.

References

[1] J. L. Volakis, A. Chatterjee, and L. C. Kempel, *Finite Element Method for Electromagnetics*, IEEE Press, New York, 1998.

[2] J.-M. Jin, *The Finite Element Method in Electromagnetics*, John Wiley & Sons, New York, 2002.

[3] A. Bossavit, *Computational Electromagnetism. Variational Formulations, Complementarity, Edge Elements*, Academic Press, San Diego, 1998.

[4] T. Weiland, "On the unique numerical solution of Maxwellian eigenvalue problems in three dimensions," *Particle Accelerators*, vol. 17, pp. 227-242, 1985.

[5] M. Clemens and T. Weiland, "Discrete electromagnetics: Maxwell's equations tailored to numerical simulations," *ICS Newsletter*, vol. 8, no. 1, pp. 5-12, 2001.

[6] C. Christopoulos, *The Transmission-Line Modeling (TLM) Method*, IEEE Press, New York, 1995.

[7] K. S. Kunz and R. J. Luebbers, *The Finite Difference Time Domain Method for Electromagnetics*, CRC Press, Florida, 1993.

[8] A. Taflove (ed.), *Advances in Computational Electromagnetics: The Finite-Difference Time-Domain Method*, Artech House, Boston, 1998.

[9] J.-F. Lee, R. Palandech, and R. Mittra, "Modeling three-dimensional discontinuities in waveguides using non-orthogonal FDTD algorithm," *IEEE Trans. Microwave Theory Tech.*, vol. 40, no. 2, pp. 346-352, 1992.

[10] S. D. Gedney and F. Lansing, "A parallel planar generalized Yee algorithm for the analysis of microwave circuit devices," *Int. J. Num. Modeling: EDNF*, vol. 8, pp. 249-263, 1995.

[11] I. J. Craddock and C. J. Railton, "Analysis of curved and angled surfaces on a Cartesian mesh using a novel finite-difference time-domain algorithm," *IEEE Trans. Microwave Theory Tech.*, vol. 43, no. 10, pp. 2460-2465, 1995.

[12] N. K. Madsen, "Divergence preserving discrete surface integral methods for Maxwell's curl equations using non-orthogonal unstructured grids," *J. Comp. Physics*, vol. 119, pp. 34-45, 1995.

[13] H. Shi and J. L. Drewniak, "Dispersion comparison for DSI- and tensor-based nonorthogonal FDTD. *IEEE Microwave Guided Wave Lett.*, vol. 6, no. 5, pp. 193-195, 1996.

[14] M. Feliziani and F. Maradei, "Mixed finite-difference/Whitney-elements time domain (FD/WE-TD) method," *IEEE Trans. Magn.*, vol. 34, no. 5, pp. 3222-3227, 1998.

[15] R. Schuhmann and T. Weiland, "FDTD on nonorthogonal grids with triangular fillings," *IEEE Trans. Magn.*, vol. 35, no. 3, pp. 1470-1473, 1999.

[16] J.-P. Berenger, "A perfectly matched layer for the absorption of electromagnetic waves," *J. Comp. Physics*, vol. 114, pp. 185-200, 1994.

[17] F. L. Teixeira and W. C. Chew, "PML-FDTD in cylindrical and spherical grids," *IEEE Microwave Guided Wave Lett.*, vol 7, no. 9, pp. 285-287, 1997.

[18] F. Collino and P. Monk, "The perfectly matched layer in curvilinear coordinates," *SIAM J. Sci. Comp.*, vol. 19, no. 6, pp. 2061-2090, 1998.

[19] P. G. Petropoulos, L. Zhao, and A. C. Cangellaris, "A reflectionless sponge layer absorbing boundary condition for the solution of Maxwell's equations with high-order staggered finite difference schemes," *J. Comp. Physics*, vol. 139, pp. 184–208, 1998.

[20] J. A. Roden and S. D. Gedney, "Efficient implementation of the uniaxial-based PML media in three-dimensional nonorthogonal coordinates with the use of the FDTD technique," *Microwave Opt. Tech. Lett.*, vol. 14, no. 2, pp. 71-75, 1997.

[21] P. G. Petropoulos, "Reflectionless sponge layers as absorbing boundary conditions for the numerical solution of Maxwell's equations in rectangular, cylindrical and spherical coordinates," *SIAM J. App. Math.*, vol. 60, no. 3, pp. 1037-1058, 2000.

[22] J. Fang, *Time-Domain Finite-Difference Computations for Maxwell's Equations*, Ph.D. dissertation, EECS Dept., University of California, Berkeley, 1989.

[23] M. F. Hadi and M. Piket-May, "A modified FDTD (2,4) scheme for modeling electrically large structures with high-phase accuracy," *IEEE Trans. Antennas Propagat.*, vol. 45, no. 2, pp. 254-264, 1997.

[24] J. L. Young, D. Gaitonde, and J. S. Shang, "Toward the construction of a fourth-order difference scheme for transient EM wave simulation: Staggered grid approach," *IEEE Trans. Antennas Propagat.*, vol. 45, no. 11, pp. 1573-1580, 1997.

[25] K. Lan, Y. Liu, and W. Lin, "A higher order (2,4) scheme for reducing dispersion in FDTD algorithms," *IEEE Trans. Electromagn. Compat.*, vol. 41, no. 2, pp. 160-165, 1999.

[26] A. Yefet and P. G. Petropoulos, "A staggered fourth-order accurate explicit finite difference scheme for the time-domain Maxwell's equations," *J. Comp. Physics*, vol. 168, pp. 286-315, 2001.

[27] S. V. Georgakopoulos, C. R. Birtcher, C. A. Balanis, and R. A. Renaut, "Higher-order finite-difference schemes for electromagnetic radiation, scattering, and penetration, parts i & ii., *IEEE Antennas Propagat. Mag.*, vol. 44, no. 1 & 2, 2002.

[28] H. Whitney, *Geometric Integration Theory*, Princeton University Press, Princeton, 1957.

[29] G. A. Deschamps, "Electromagnetics and differential forms," *Proc. IEEE*, vol. 69, no. 6, pp. 676-696, 1981.

[30] W. L. Burke, *Applied Differential Geometry*, Cambridge University Press, 1985.

[31] P. Hammond and J. K. Sykulski, *Engineering Electromagnetism*: *Physical Processes and Computation*, Oxford University Press, Oxford, 1994.

[32] E. Tonti, "On the geometrical structure of electromagnetism," in *Gravitation, Electromagnetism and Geometrical Structures* (G. Ferarese, ed.), pp. 281-308, 1995.

[33] J. K. Sykulski (ed.), *Computational Magnetics*, Chapman & Hall, Suffolk, 1995.

[34] D. Baldomir and P. Hammond, *Geometry of Electromagnetic Systems*, Clarendon Press, Oxford, 1996.

[35] F. L. Teixeira and W. C. Chew, "Differential forms, metrics, and the reflectionless absorption of electromagnetic waves," *J. Electromagn. Waves Applicat.*, vol. 13, no. 5, pp. 665-686, 1999.

[36] R. Hiptmair, *Discrete Hodge operators*, Tech. Rep. 126, SFB 382, Univ. Tubingen, Germany, 1999.

[37] F. L. Teixeira and W. C. Chew, "Lattice electromagnetic theory from a topological point of view," *J. Math. Physics*, vol. 40, no. 1, pp. 169-187, 1999.

[38] A. Bossavit and L. Kettunen, "Yee-like schemes on a tetrahedral mesh, with diagonal lumping," *Int. J. Num. Modeling: ENDF*, vol. 12, pp. 129-142, 1999.

[39] F. L. Teixeira and W. C. Chew, "Differential forms, metrics, and the reflectionless absorption of electromagnetic waves," *J. Electromagn. Waves Applicat.*, vol. 13, no. 5, pp. 665-686, 1999.

[40] C. Mattiussi, "The finite volume, finite element and finite difference methods as numerical methods for physical field problems," in *Advances in Electronics and Electron Physics* (P. Hawkes, ed.), vol. 113, pp. 1-146, 2000.

[41] E. Tonti, "Finite formulation of electromagnetic field," *ICS Newletter*, vol. 8, no. 1, pp. 5-11, 2001.

[42] R. E. Mickens, *Nonstandard Finite Difference Models of Differential Equations*, World Scientific, Singapore, 1994.

[43] J. B. Cole, "A high-accuracy realization of the Yee algorithm using non-standard finite differences," *IEEE Trans. Microwave Theory Tech.*, vol. 45, no. 6, pp. 991-996, 1997.

[44] N. V. Kantartzis and T. D. Tsiboukis, "A generalized methodology based on higher-order conventional and nonstandard FDTD concepts for the systematic development of enhanced dispersionless wide-angle absorbing PMLs," Int. J. Numeric. Modeling: ENDF, vol. 12, pp. 417-440, 2000.

[45] T. Kashiwa, H. Kudo, Y. Sendo, T. Ohtani, and Y. Kanai, "The phase velocity error and stability condition of the three-dimensional nonstandard FDTD method," *IEEE Trans. Magn.*, vol 38, no. 2, pp. 661-664, 2002.

Nikolaos V. Kantartzis and Theodoros D. Tsiboukis
Advanced & Computational Electromagnetics Laboratory
Department of Electrical & Computer Engineering
Aristotle University of Thessaloniki, GR-54124
Greece